Quantum dynamics as a stochastic process

Sarah John
Vigyan, Inc., 30 Research Drive, Hampton, Virginia 23666-1325

John W. Wilson
NASA Langley Research Center, Hampton, Virginia 23681-0001
(Received 19 July 1993)

The quantum Liouville equation is solved in the Wigner representation using generalized Monte Carlo techniques. For small increments of time, the solution is represented as a sequential classical evolution in phase space followed by a quantum "jump" distribution in momentum space, with the latter simulated via a stochastic method. Extending the work initiated by John and Remler [Ann Phys. (N.Y.) **180**, 152 (1987)] the technique is developed and validated for higher dimensions. Also, an alternative algorithm is developed and applied to study motion of a quantum system in an anharmonic quartic potential well, with significantly improved results.

PACS number(s): 05.30.−d

I. INTRODUCTION

The density operator formalism of quantum dynamics [1] provides a suitable framework for the study of thermodynamical systems. The dynamical equation for the density operator, given by the quantum Liouville equation, translates into ordinary functions and derivatives of phase space coordinates in the Wigner representation [2–5]. In a series expansion, the equation can be shown to reduce to the classical Liouville equation and is therefore a very suitable representation for revealing purely quantum effects. Also, the more familiar equations appearing in nuclear scattering theory, such as the hydrodynamical equations [3,6] and the Boltzmann-Vlasov equations [7] may be extracted from the Wigner formalism under certain approximations [3].

In this paper, Monte Carlo techniques are applied to solve the quantum Liouville equation in the Wigner representation [9,10]. The equation is in a noncovariant form, and applies to single-particle dynamics only. The time evolution is treated as a stochastic process [5,8–10]. (Does nature indeed play dice?) To simplify the problem only first-order quantum effects will be considered, and in this approximation the solution is applicable to quasiclassical systems [9–12] that exhibit smoothly varying momentum distribution typical of highly mixed thermodynamical systems. In general, however, first-order quantum correction may not be sufficient, and in some instances it even requires the entire series summation [13]. For scattering of a highly collimated beam, for example, higher-order terms become increasingly significant.

A generalized Monte Carlo method was introduced in Refs. [9,10]. This paper extends the work to two and three dimensions, and an alternative algorithm is developed which gives improved results for the application considered.

In Sec. II quantum dynamics in the Wigner representation is reviewed, and the stochastic techniques developed. In Sec. III the technique is validated independently of the classical motion by comparison with analytic solutions in the one-, two-, and three-dimensional momentum space. In Sec. IV an application to bound-state motion within an anharmonic quartic potential in two-dimensional phase space is considered and the algorithm discussed. In Sec. V results and discussions are presented.

II. THEORY

A. Quantum Liouville equation (QLE)

The density operator $\hat{\rho}$ of a quantum thermodynamical system is given by

$$\hat{\rho}=\sum_m P_m|\psi_m\rangle\langle\psi_m| , \tag{1}$$

where P_m is the probability for an ensemble element to be in the eigenstate $|\psi_m\rangle$. The time evolution of $\hat{\rho}$ is the quantum Liouville equation,

$$i\frac{\partial\hat{\rho}}{\partial t}=[\hat{H},\hat{\rho}] , \tag{2}$$

where $\hat{H}$ is the Hamiltonian ($\hbar=1$) and has the formal solution

$$\hat{\rho}(t)=e^{-i\hat{H}t}\hat{\rho}(0)e^{i\hat{H}t} . \tag{3}$$

The components of $\hat{H}$ in general being noncommutative, this form is difficult to solve in practice. An intuitively appealing form is obtained by taking the Wigner transform of the QLE, which in the classical limit reduces to the classical Liouville equation.

B. Wigner representation of the QLE

A few basic properties of the Wigner transform are now reviewed. The Wigner transform of an operator $\hat{O}$ is defined by

$$O_W(\mathbf{x},\mathbf{p},t)=\int_{-\infty}^{\infty}d\mathbf{y}\,e^{i\mathbf{p}\cdot\mathbf{y}}\langle\mathbf{x}-\tfrac{1}{2}\mathbf{y}|\hat{O}(t)|\mathbf{x}+\tfrac{1}{2}\mathbf{y}\rangle , \tag{4}$$

which is a simultaneous representation in both position coordinates $\mathbf{x}$ and momentum coordinates $\mathbf{p}$. The Wigner transform for the density operator $\hat{\rho}$ is

$$f_W(\mathbf{x},\mathbf{p},t)=\int_{-\infty}^{\infty} d\mathbf{y}\, e^{i\mathbf{p}\cdot\mathbf{y}}\langle \mathbf{x}-\tfrac{1}{2}\mathbf{y}|\hat{\rho}(t)|\mathbf{x}+\tfrac{1}{2}\mathbf{y}\rangle \ , \tag{5}$$

and is called the Wigner distribution function [generally defined with a normalization factor $(2\pi)^{-3}$]. As an example, the Wigner transform of the density operator corresponding to a minimum wave packet,

$$\psi(\mathbf{x})=\frac{1}{(2\pi\sigma^2)^{3/2}} e^{-i\mathbf{p}_0\cdot\mathbf{x}-(\mathbf{x}-\mathbf{x}_0)^2/4\sigma^2} \ , \tag{6}$$

is given by

$$\begin{aligned} f_W(\mathbf{x},\mathbf{p},t)&=\int_{-\infty}^{\infty} d\mathbf{y}\, e^{i\mathbf{p}\cdot\mathbf{y}}\psi^*(\mathbf{x}-\tfrac{1}{2}\mathbf{y})\psi(\mathbf{x}+\tfrac{1}{2}\mathbf{y}) \\ &=2e^{-2\sigma^2(\mathbf{p}-\mathbf{p}_0)^2-(\mathbf{x}-\mathbf{x}_0)^2/2\sigma^2} \ . \end{aligned} \tag{7}$$

The Wigner function has many analogs with the classical distribution function. For example,

$$(2\pi)^{-3}\int d\mathbf{p}\, f_W(\mathbf{x},\mathbf{p},t)=\langle \mathbf{x}|\hat{\rho}|\mathbf{x}\rangle \ , \tag{8}$$

$$(2\pi)^{-3}\int d\mathbf{x}\, f_W(\mathbf{x},\mathbf{p},t)=\langle \mathbf{p}|\hat{\rho}|\mathbf{p}\rangle \ , \tag{9}$$

$$(2\pi)^{-3}\int d\mathbf{x}\, d\mathbf{p}\, f_W(\mathbf{x},\mathbf{p},t)=1 \ , \tag{10}$$

and the expectation value of an observable $\hat{O}$ is given by

$$\langle \hat{O}(t)\rangle=(2\pi)^{-3}\int d\mathbf{x}\, d\mathbf{p}\, O_W(\mathbf{x},\mathbf{p},t) f_W(\mathbf{x},\mathbf{p},t) \ . \tag{11}$$

However, $f_W(\mathbf{x},\mathbf{p},t)$, even though real, $f_W^*=f_W$, is not strictly a distribution function since it can have negative values. Therefore the Wigner function should at most be considered an auxiliary function useful for calculating thermodynamical averages.

The Wigner transform of the quantum Liouville equation becomes

$$\frac{\partial f_W}{\partial t}(\mathbf{x},\mathbf{p},t)=-2H_W \sin\left|\frac{\Lambda}{2}\right| f_W(\mathbf{x},\mathbf{p},t) \ , \tag{12}$$

where H_W is the Wigner transformed Hamiltonian, and Λ is the Poisson bracket operator,

$$\Lambda=\overleftarrow{\nabla}_{\mathbf{p}}\cdot\overrightarrow{\nabla}_{\mathbf{x}}-\overleftarrow{\nabla}_{\mathbf{x}}\cdot\overrightarrow{\nabla}_{\mathbf{p}} \ , \tag{13}$$

the arrows indicating the direction of action of the operator. Expanding the sine term, the following series expansion is obtained:

$$\begin{aligned} \frac{\partial f_W}{\partial t}(\mathbf{x},\mathbf{p},t)&=[-H_W\Lambda+\tfrac{1}{24}H_W\Lambda^3 \\ &\quad -\tfrac{1}{1920}H_W\Lambda^5+\cdots]f_W(\mathbf{x},\mathbf{p},t) \\ &=-(\mathcal{L}_c+\mathcal{L}_q)f_W(\mathbf{x},\mathbf{p},t) \ , \end{aligned} \tag{14}$$

where $\mathcal{L}_c=H_W\Lambda$ is the classical Liouville operator and $\mathcal{L}_q$ (= all higher-order terms) is the quantum jump operator. The solution to Eq. (14) is given by

$$f_W(\mathbf{x},\mathbf{p},t)=e^{-(\mathcal{L}_c+\mathcal{L}_q)t} f_W(\mathbf{x},\mathbf{p},0) \ . \tag{15}$$

For small increments of time, to $O(\Delta t^2)$,

$$f_W(\mathbf{x},\mathbf{p},\Delta t)=e^{-\mathcal{L}_q\Delta t}e^{-\mathcal{L}_c\Delta t} f_W(\mathbf{x},\mathbf{p},0) \ . \tag{16}$$

Hence infinitesimal time motion can be described in terms of successive classical and quantum evolutions, where the classical operator transforms the function to

$$f_{Wc}(\mathbf{x},\mathbf{p},\Delta t)=e^{-\mathcal{L}_c\Delta t} f_W(\mathbf{x},\mathbf{p},0) \ , \tag{17}$$

and the quantum jump operator acts on f_{Wc}, giving

$$f_W(\mathbf{x},\mathbf{p},\Delta t)=e^{-\mathcal{L}_q\Delta t} f_{Wc}(\mathbf{x},\mathbf{p},\Delta t) \ . \tag{18}$$

Explicit expressions for the operators $\mathcal{L}_c$ and $\mathcal{L}_q$ for a Hamiltonian operator of the form

$$\hat{H}=\frac{\hat{\mathbf{p}}^2}{2m}+V(\hat{\mathbf{x}}) \tag{19}$$

with Wigner transform

$$H_W(\mathbf{x},\mathbf{p})=\frac{\mathbf{p}^2}{2m}+V(\mathbf{x}) \ , \tag{20}$$

where $\mathbf{x}$ and $\mathbf{p}$ are now variables and not operators, are obtained as

$$\mathcal{L}_c=\frac{\mathbf{p}}{m}\cdot\vec{\nabla}_{\mathbf{x}}-(\vec{\nabla}_{\mathbf{x}}V)\cdot\vec{\nabla}_{\mathbf{p}} \ , \tag{21}$$

$$\mathcal{L}_q=\tfrac{1}{24}V(\mathbf{x})(\vec{\nabla}_{\mathbf{x}}\cdot\vec{\nabla}_{\mathbf{p}})^3+\cdots \ . \tag{22}$$

The expressions (17) and (18) are difficult to evaluate analytically for arbitrary functions. Hence Monte Carlo techniques are applied which have the advantage that the only analytic evaluation required is that for the action of the operators on a δ function.

C. Monte Carlo method

In a Monte Carlo procedure an importance sample set of test points is selected to represent the initial positive-valued Wigner function

$$f_W(\mathbf{x},\mathbf{p},0)\approx\frac{(2\pi)^3}{N}\sum_{i=1}^{N}\sigma_i\delta(\mathbf{x}-\mathbf{x}_i)\delta(\mathbf{p}-\mathbf{p}_i) \ , \tag{23}$$

where $\sigma_i=1$ is the sign of the test point, since, as noted above, $f_W(\mathbf{x},\mathbf{p},t)$ may be positive or negative and the factor $(2\pi)^3$ is included to satisfy the normalization given by Eq. (10). It must be emphasized that in quantum mechanics the Wigner distribution function $f_W(x,p,0)$ itself cannot be a δ function due to the inherent uncertainty relations [14]. In applications considered here, the initial distribution function satisfies the uncertainty relations $\Delta x\,\Delta p\geq\frac{1}{2}$, see Eq. (65). The decomposition of the initial state into δ functions as given by Eq. (23) is merely a mathematical convenience, with equality defined by the general representation

$$g(x)=\int g(x')\delta(x-x')dx' \ .$$

The classical propagation is a canonical contact transformation, which transports the δ functions to new positions along deterministic trajectories,

$$f_{Wc}(\mathbf{x},\mathbf{p},\Delta t)=\frac{(2\pi)^3}{N}\sum_i \sigma_i e^{-\mathcal{L}_c\Delta t}\delta(\mathbf{x}-\mathbf{x}_i)\delta(\mathbf{p}-\mathbf{p}_i)$$
$$=\frac{(2\pi)^3}{N}\sum_i \sigma_i\delta(\mathbf{x}-\mathbf{x}_{ci})\delta(\mathbf{p}-\mathbf{p}_{ci}) , \quad (24)$$

where $\mathbf{x}_{ci}$ and $\mathbf{p}_{ci}$ are evaluated via Hamilton's equations of motion,

$$\frac{d\mathbf{x}_i}{dt}=\frac{\partial H}{\partial \mathbf{p}_i} ,$$
$$\frac{d\mathbf{p}_i}{dt}=-\frac{\partial H}{\partial \mathbf{x}_i} . \quad (25)$$

The quantum correction is given by

$$f_W(\mathbf{x},\mathbf{p},\Delta t)=\frac{(2\pi)^3}{N}\sum_i \sigma_i e^{-\mathcal{L}_q\Delta t}\delta(\mathbf{x}-\mathbf{x}_{ci})\delta(\mathbf{p}-\mathbf{p}_{ci}) . \quad (26)$$

The action of $\mathcal{L}_q$ on the δ function is now evaluated explicitly in the quasiclassical limit for a central potential $V(r)$ with $r=|\mathbf{x}-\mathbf{x}_i|$ and

$$\mathcal{L}_q=\tfrac{1}{24}V(r)(\overleftarrow{\nabla}_{\mathbf{x}}\cdot\vec{\nabla}_{\mathbf{p}})^3 . \quad (27)$$

Expanding $\mathcal{L}_q$ in terms of the radial component p_0, and perpendicular components p_1,p_2 (Appendix A), gives [10]

$$\mathcal{L}_q=\mathcal{L}_{q1}+\mathcal{L}_{q2} ,$$

where

$$\mathcal{L}_{q1}=\frac{a_L}{2}\partial^3_{p_0}+a_T\partial_{p_0}\partial^2_{p_1} , \quad (28)$$

$$\mathcal{L}_{q2}=\frac{a_L}{2}\partial^3_{p_0}+a_T\partial_{p_0}\partial^2_{p_2} , \quad (29)$$

with

$$a_L=\frac{1}{24}\frac{\partial^3 V}{\partial r^3} , \quad (30)$$

$$a_T=\frac{1}{8}\frac{\partial}{\partial r}\left[\frac{1}{r}\frac{\partial V}{\partial r}\right] . \quad (31)$$

Consider first the action of $\mathcal{L}_{q1}$ on the δ function. (Similar arguments hold for $\mathcal{L}_{q2}$.) It acts on the p_0 and p_1 components only, giving

$$\mathcal{J}(\mathbf{p}-\mathbf{p}_i)=e^{-\mathcal{L}_{q1}t}\delta(\mathbf{p}-\mathbf{p}_i)$$
$$=\delta(p_2-p_{2i})e^{-\mathcal{L}_{q1}t}\delta(p_0-p_{0i})\delta(p_1-p_{1i}) . \quad (32)$$

A change of variables to $v_0=p_0+\gamma p_1$ and $v_1=p_0-\gamma p_1$, with

$$\gamma=\left[\frac{3a_L}{2a_T}\right]^{1/2} , \quad (33)$$

transforms $\mathcal{L}_{q1}$ into

$$\mathcal{L}_{q1}=a\partial^3_{v_0}+a\partial^3_{v_1} , \quad (34)$$

where

$$a=\frac{a_L}{2}+a_T\gamma^2=2a_L \quad (35)$$

and Eq. (32) transforms into

$$\mathcal{J}(\mathbf{p}-\mathbf{p}_i)\rightarrow 2\gamma\delta(p_2-p_{2i})e^{-at\partial^3_{v0}}$$
$$\times\delta(v_0-v_{0i})e^{-at\partial^3_{v1}}\partial(v_1-v_{1i}) , \quad (36)$$

where 2γ is the Jacobian of the transformation for the δ functions.

The expressions to be evaluated are of the typical one-dimensional form. With the factor t integrated into a,

$$\mathrm{Ai}(a;p-p_i)=e^{-a\partial^3_p}\delta(p-p_i)$$
$$=\frac{1}{2\pi}\int_{-\infty}^{\infty}dy\, e^{iay^3+ipy} , \quad (37)$$

where Ai is recognized as the Airy function. Depending on the sign of a, the function decreases exponentially along one direction and is oscillatory along the other, with a slow decay in amplitude and increasing frequency. Hence the quantum jump operator gives a nonlocal momentum dependence to the δ function, and the concept of deterministic motion becomes untenable.

To incorporate the quantum correction into a Monte Carlo scheme, a faster damping rate for the Airy functions is useful to speed simulation. (Details for only the one-dimensional quantum correction are discussed here. For higher dimensions see Sec. III.) Now the phase space assumes a graininess due to the δ function representation; the larger the number of representative points, the finer the grain structure. For a coarse-grained analysis of the quantum correction, the increasing rapidity of the oscillation of the Airy function at large momentum distances implies an average cancellation. Hence a grain size is introduced into the $\delta(p-p_i)$, producing a faster damping rate for the function. This is achieved by approximating the δ function by a narrow-width Gaussian function, which modifies the Airy function to

$$\mathcal{J}_\alpha(a;p-p_i)=e^{-a\partial^3_p}\delta_\alpha(p-p_i) , \quad (38)$$

where $\delta_\alpha(p-p_i)$ is the Gaussian function of width α. The expressions for the modified Airy functions $\mathcal{J}_\alpha$ are given in Appendix B.

The corresponding quantum jump function is defined as

$$J_\alpha(a;p-p_i)=\mathcal{J}_\alpha(a;p-p_i)-\delta_\alpha(p-p_i) . \quad (39)$$

Figure 1(a) illustrates a typical Gaussian modified Airy function and Fig. 1(b) the corresponding quantum jump function.

The jump function is implemented as a stochastic process. To this end, let $J_\pm$ correspond to the positive and negative segments of the function J_α. It can be easily shown by partial integration,

$$\int J_\alpha(a;p-p_i)dp=0 , \quad (40)$$

which indicates that the areas under the positive and neg-

ative segments are equal. Defining the area A,

$$A = \int |J_{\pm}| dp \ , \tag{41}$$

and rewriting

$$J_{\alpha}(a;p-p_i) = A \left[\frac{|J_+|}{A} - \frac{|J_-|}{A} \right] = A\,[F_+ - F_-] \ , \tag{42}$$

defines the jump "probability" functions, $F_{\pm}(a;p-p_i) = |J_{\pm}|/A$.

The stochastic process is based on the following probabilistic interpretation. For two random variables X and Y the joint probability $P(X,Y)$ is given by

$$P(X,Y) = P(X|Y)P(Y) \ , \tag{43}$$

where $P(Y)$ is the probability for the event Y and $P(X|Y)$ is the conditional probability for the event X, provided event Y has occurred. Compare now with Eq. (42). If $A < 1$, interpret $P(Y) = A$ as the probability for the quantum event, or the creation probability. In other words, not all test points undergo quantum events during each time interval, but only those selected randomly with probability $P(Y)$. Generally, a is small enough (see Fig. 2) to ensure that $A < 1$, so that at most one quantum event occurs per time step.

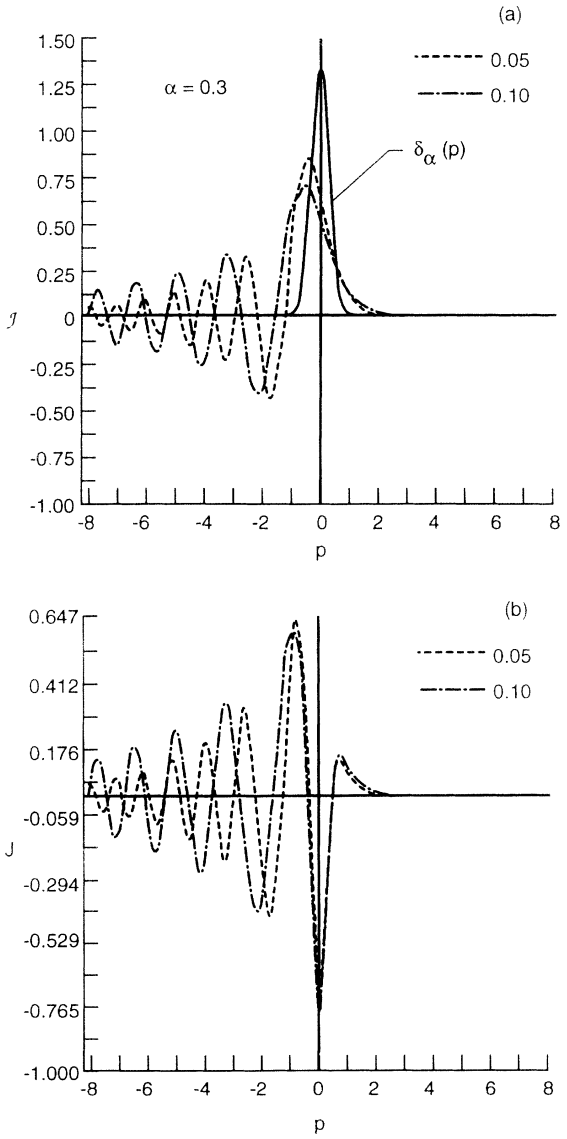

FIG. 1. (a) Damped Airy functions, $\delta_{\alpha}(a;p)$ for $a = 0.05, 0.1$; $\alpha = 0.3$. (b) The jump function $J_{\alpha}(a;p)$ corresponding to Fig. (a).

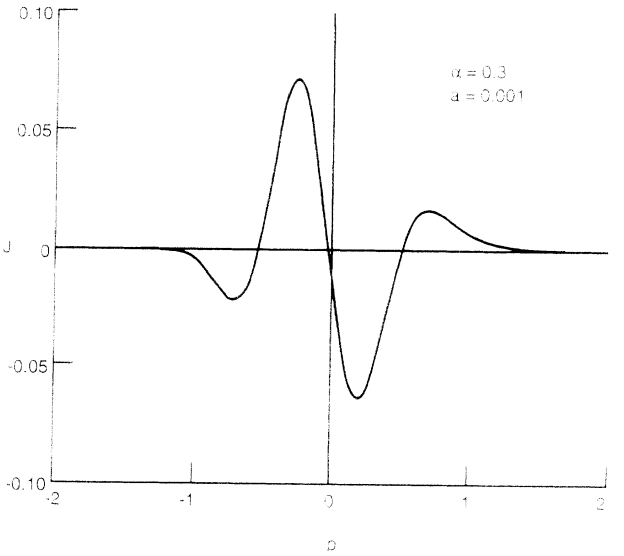

FIG. 2. Jump function $J_{\alpha}(a;p)$ for very small increments of time, $a = 0.001$, $\alpha = 0.3$.

The conditional probability $P(X|Y) = F_+ - F_-$ represents the momentum jump probability functions corresponding to the random variable $X \equiv p$. A pair of values $\Delta p_{\pm}$ is selected randomly using the cumulative distributions for $F_{\pm}$. In the Monte Carlo representation, this becomes a test pair with coordinates,

$$\delta(p - (p_{ci} + \Delta p_{\pm}))\delta(x - x_{ci})\sigma_i \sigma_{\pm} \ , \tag{44}$$

where $\sigma_{\pm} = \pm 1$ for the positive and negative points. The newly created points are appended to the initial set to undergo subsequent classical and quantum motions. If $A \ll 1$, a factor M is introduced to enhance the creation probability to MA, with a normalization factor $1/M$ for the new pairs.

Clearly, in the absence of the classical motion, the stochastic process is a Markoff process. That is, with $t_{n-1} < t_n$,

$$F\{p(t_n) \le p_n | p(t), t \le t_{n-1}\} = F\{p(t_n) \le p_n | p(t_{n-1})\} \ .$$

The jump probability for each test point is thus independent of its past histories, and depends only on its present location in momentum space.

III. VALIDATION OF STOCHASTIC QUANTUM JUMP MOTION

The validity of the technique developed in the previous section is established by comparing stochastic quantum time development in momentum space with analytic solu-

tions. This is easily done when the initial function is a Gaussian.

A. One-dimensional momentum space

The quantum time development for the interval t in the quasiclassical approximation is given by

$$f(p,t)=e^{-at\partial_p^3}f(p,0)\ . \tag{45}$$

With the initial function

$$f(p,0)=\frac{1}{\sqrt{2\pi}\alpha}e^{-p^2/2\alpha^2}\ , \tag{46}$$

the analytic solution is the Gaussian modified Airy function given in Appendix B.

For the stochastic evolution a representative set of points for the initial function is chosen as follows. A pair of values (p_i,f_i) is selected randomly within a specified boundary for f and p such that the function f lies well within the defined area. f varies from 0 to $f_{\max}=1/(\sqrt{2\pi}\alpha)$. If $f(p_i)<f_i$, then p_i is selected; otherwise it is discarded. Hence

$$f(p,0)\approx\frac{1}{N}\sum_{i=1}^{N}\delta_{\alpha'}(p-p_i)\ , \tag{47}$$

where the test Gaussian functions have width α', with $\alpha'\ll\alpha$. Dividing the total time t into K discrete time intervals ($\Delta t=t/K$), the time development is written as

$$f(p,t)=[e^{-a\Delta t\partial_p^3}]^K f(p,0)\ . \tag{48}$$

During each time step, statistical test points are selected with probability A [see discussion following Eq. (42)] and new test pairs created at $p_i+\Delta p_\pm$, where $\Delta p_\pm$ are selected with conditional probability $F_\pm$, which get appended to the main set. The updated set is propagated in the subsequent time interval.

In the actual algorithm, the momentum space is divided into grids, and the test points assigned on it. With $at=0.1$ and $a\Delta t=0.001$, 100 time steps are executed, and at the end of the run the function is reconstructed from the test points using harmonic-oscillator functions [9]. If $A\ll 1$, the creation probability is enhanced by an arbitrary factor M set at $M=10\,000/N$. Thus for 100 initial points the creation probability is increased 100 times. Each representative pair for $J_{\alpha'}(a\Delta t;p-p_i)$ is therefore given by

$$\frac{1}{M}[\delta(p-(p_i+\Delta p_+))-\delta(p-(p_i+\Delta p_-))]\ . \tag{49}$$

For a density k on the grids, the process is repeated k times.

Figures 3(a) and 3(b) compare the results with the analytic solutions for various grid size, initial number of test points N, and for various Gaussian widths α' for the test points. The results show good agreement with the analytic solutions and appear to be independent of the variables.

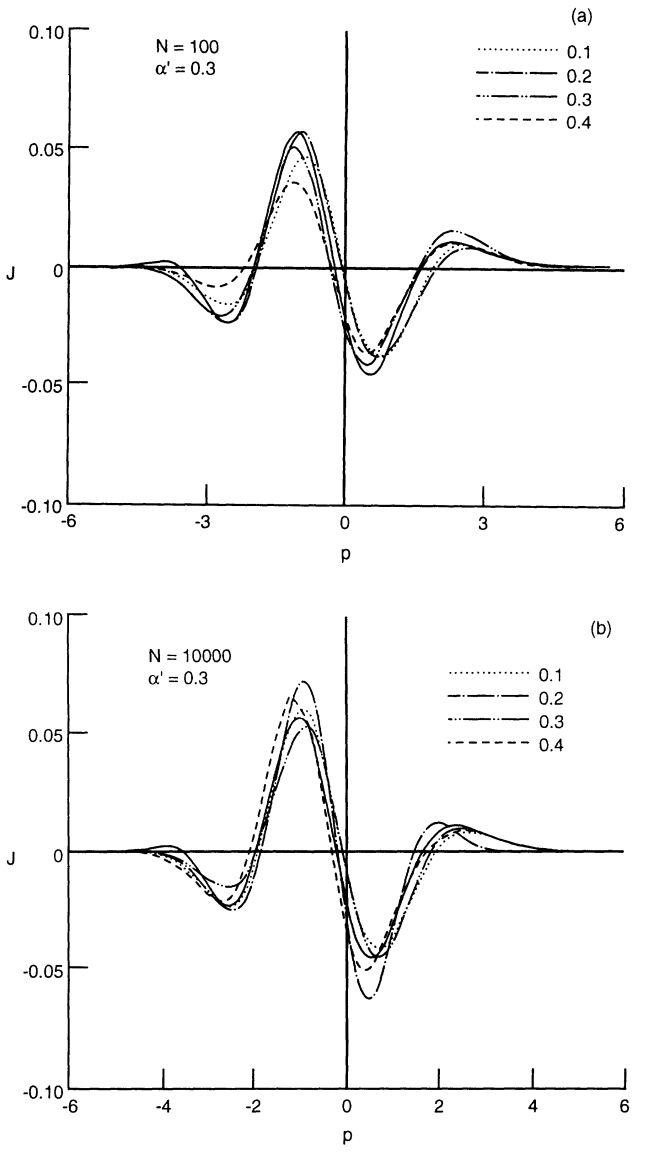

FIG. 3. Stochastic evolution of jump function after 100 time steps compared with analytic solution (solid line), $J_\alpha(a;p)$, $a=0.1$, $\alpha=1$, for varying grid sizes, 0.1, 0.2, 0.3, 0.4. Initial number of test points (a) $N=100$, (b) 10000, with width $\alpha'=0.3$.

B. Two-dimensional momentum space

The two-dimensional quantum jump motion is given by

$$f(p_0,p_1,t)=e^{-\mathcal{L}_q t}f(p_0,p_1,0)\ , \tag{50}$$

where p_0,p_1 are the radial and perpendicular components and $\mathcal{L}_q$ is given by Eq. (28) with $a_L/2$ replaced by a_L. The initial function is chosen to be

$$f(p_0,p_1,0)=\frac{1}{2\pi\alpha^2}e^{-(p_0^2+p_1^2)/2\alpha^2}\ . \tag{51}$$

To obtain the analytic solution, change variables to $v_0=p_0+p_1$, $v_1=p_0-p_1$,

$$\tilde{f}(v_0,v_1,t)=\frac{1}{2\pi\alpha^2}[e^{-at\partial^3_{v_0}}e^{-v_0^2/4\alpha^2}] \times[e^{-at\partial^3_{v_1}}e^{-v_1^2/4\alpha^2}] , \tag{52}$$

which is recognized as a product of one-dimensional forms. The inverse transformation is then computed to get the analytic solution.

For the stochastic evolution, consider the action of $\mathcal{L}_q$ on a test point during the subinterval Δt given by

$$\mathcal{J}(a\Delta t;\mathbf{p}-\mathbf{p}_i)=e^{-\mathcal{L}_q\Delta t}\delta(p_0-p_{0i})\delta(p_1-p_{1i}) . \tag{53}$$

Transforming to variables v_0 and v_1 as before, together with a Gaussian width α' for the transformed test points,

$$\mathcal{J}(a\Delta t;\mathbf{p}-\mathbf{p}_i)\rightarrow 2[e^{-a\Delta t\partial^3_{v_0}}\delta_{\alpha'}(v_0-v_{0i})][e^{-a\Delta t\partial^3_{v_1}}\delta_{\alpha'}(v_1-v_{1i})]$$
$$=2[J_{\alpha'}(v_0-v_{0i})+\delta_{\alpha'}(v_0-v_{0i})][J_{\alpha'}(v_1-v_{1i})+\delta_{\alpha'}(v_1-v_{1i})] , \tag{54}$$

which to $O(\Delta t)$ gives

$$\mathcal{J}(a\Delta t;\mathbf{p}-\mathbf{p}_i)\rightarrow 2[e^{-a\Delta\partial^3_{v_0}}\delta_{\alpha'}(v_0-v_{0i})][e^{a\Delta t\partial^3_{v_1}}\delta_{\alpha'}(v_1-v_{1i})]$$
$$\approx 2[J_{\alpha'}(v_0-v_{0i})\delta_{\alpha'}(v_1-v_{1i})+J_{\alpha'}(v_1-v_{1i})\delta_{\alpha'}(v_0-v_{0i})+\delta_{\alpha'}(v_0-v_{0i})\delta_{\alpha'}(v_1-v_{1i})] , \tag{55}$$

since $J_{\alpha'}$ is of $O(\Delta t)$. The pair selection for each $J_{\alpha'}$ is done as before and the newly created representative test pairs are

$$\delta(v_1-v_{1i})\delta(v_0-(v_{0i}+\Delta v_{0\pm}))\sigma_{\pm}\sigma_i+\delta(v_0-v_{0i})\delta(v_1-(v_{1i}+\Delta v_{1\pm}))\sigma_{\pm}\sigma_i . \tag{56}$$

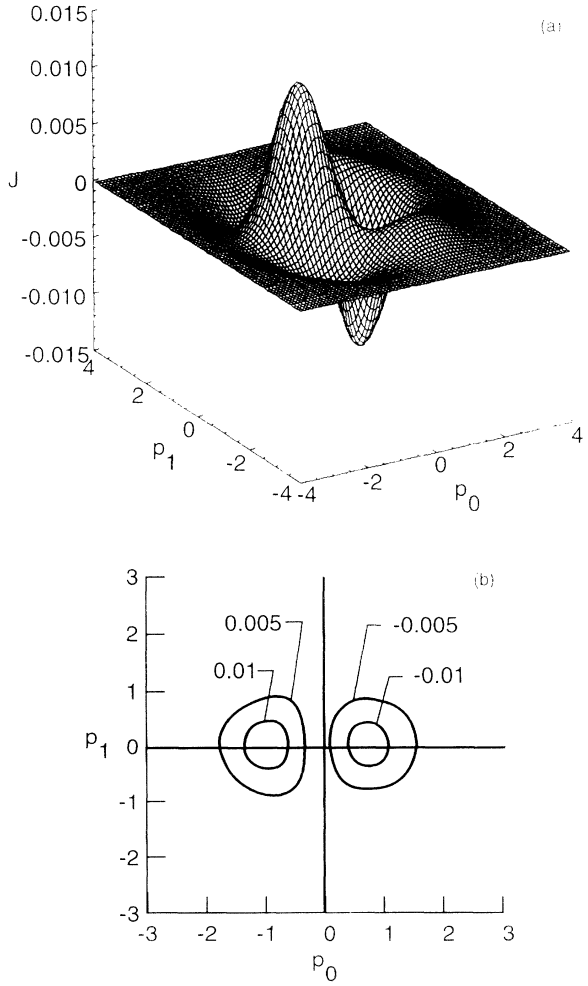

FIG. 4. (a) Analytic two-dimensional jump function $J_\alpha(a;p_0,p_1)$ with (b) contours for $a=0.1$, $\alpha=1$.

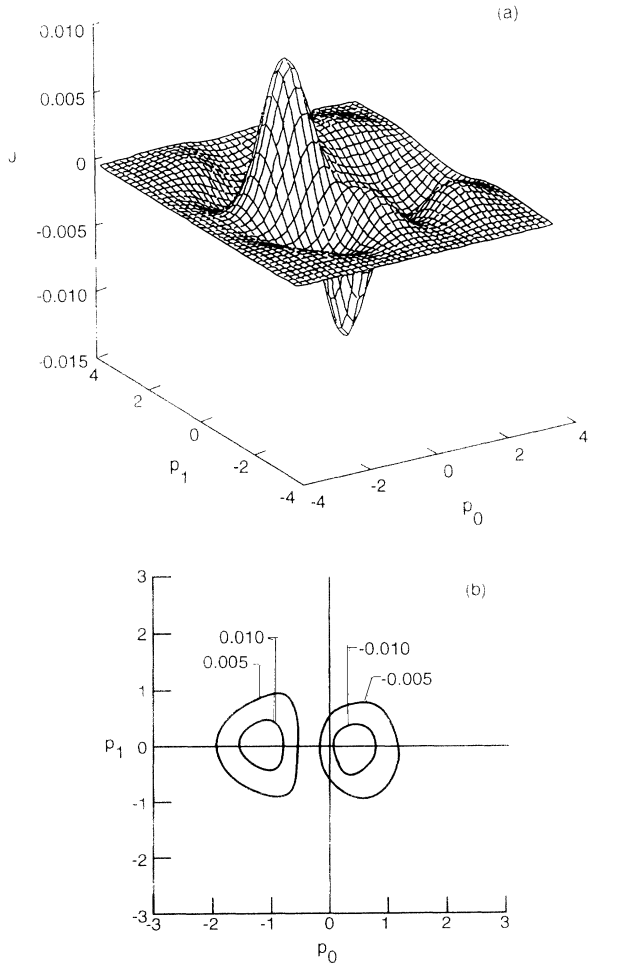

FIG. 5. (a) Stochastic evolution of jump function $J_\alpha(a;p_0,p_1)$ with (b) contours for $a=0.1$, $\alpha=1$, in two dimensions using 100 time steps, with $N=10\,000$, grid size $=0.2$, $\alpha'=0.4$.

Note that two pairs are created for each event as expressed by the summation. Transforming back to the original coordinates, the representative test pairs are

$$\delta\left[p_0-\left[p_{0i}+\frac{\Delta v_{0\pm}}{2}\right]\right]\delta\left[p_1-\left[p_{1i}+\frac{\Delta v_{0\pm}}{2}\right]\right]\sigma_{\pm}\sigma_i+\delta\left[p_0-\left[p_{0i}+\frac{\Delta v_{1\pm}}{2}\right]\right]\delta\left[p_1-\left[p_{1i}-\frac{\Delta v_{1\pm}}{2}\right]\right]\sigma_{\pm}\sigma_i\ . \tag{57}$$

Figures 4 and 5 compare the analytic results with the stochastic simulation, showing very good agreement. As before, 100 time steps were executed, and the pair creation probability was enhanced by a factor of 20 using an initial number of 10 000 points.

C. Three-dimensional momentum space

The three-dimensional jump motion is given by

$$f(\mathbf{p},t)=e^{-\mathcal{L}_q t}f(\mathbf{p},0)\ . \tag{58}$$

The initial Gaussian function may be written in terms of parallel and perpendicular components,

$$f(\mathbf{p},0)=\frac{1}{(\sqrt{2\pi}\alpha)^3}e^{-(p_0^2+\mathbf{p}_1^2)/2\alpha^2}\ . \tag{59}$$

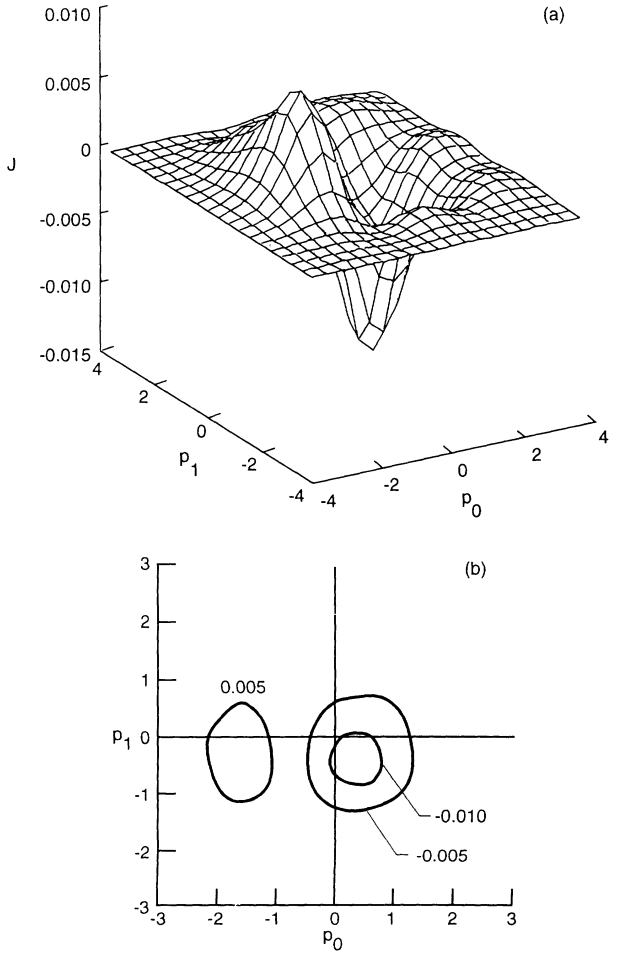

FIG. 6. (a) Stochastic evolution of jump function $J_\alpha(a;\mathbf{p})$ with (b) contours for $a=0.1$, $\alpha=1$ in three dimensions using ten time steps. The plot is for the p_0,p_1 plane. $N=10\,000$; grid size $=0.4$; $\alpha'=0.3$.

Similarly, from Appendix A,

$$\mathcal{L}_q=a_L\partial_{p0}^3+a_T\partial p_0\partial^2\mathbf{p}_\perp\ . \tag{60}$$

Hence the analytic solution is similar to the two-dimensional case on a plane defined by p_0 and $p_\perp$. For the stochastic time development, consider $\mathcal{L}_q$ acting on a test point during time interval Δt,

$$\mathcal{J}(\mathbf{p}-\mathbf{p}_i)=e^{-\mathcal{L}_{q2}\Delta t}e^{-\mathcal{L}_{q1}\Delta t}\delta(p_0-p_{0i})\times\delta(p_1-p_{1i})\delta(p_2-p_{2i})\ , \tag{61}$$

where $\mathcal{L}_{q1}$ and $\mathcal{L}_{q2}$ are given by Eqs. (28) and (29). To $O(\Delta t)$, the sample set generated by $\mathcal{L}_{q1}$ and $\mathcal{L}_{q2}$ acting simultaneously on the test point creates four new pairs.

$\mathcal{L}_{q1}$ generates two sets of pairs as in the two-dimensional case, and is written succinctly as

$$\sum_{j\neq i=1}^{2}\delta(p_0-p_{0j})\delta(p_1-p_{1j})\delta(p_2-p_{2i})\sigma_i\sigma_{j\pm}\ . \tag{62}$$

Similarly, $\mathcal{L}_{q2}$ acting on $\delta(\mathbf{p}-\mathbf{p}_i)$ generates the set

$$\sum_{j\neq i=1}^{2}\delta(p_0-p_{0j})\delta(p_2-p_{2j})\delta(p_1-p_{1i})\sigma_i\sigma_{j\pm}\ . \tag{63}$$

Figure 6 shows the results for the p_0,p_1 plane. The comparison with analytic solutions is remarkably good even with 10 000 initial points. Also by choosing $a\Delta t=0.01$, only 10 time steps are required.

IV. APPLICATION IN TWO-DIMENSIONAL PHASE SPACE

The full quantum motion, namely, the classical evolution followed by the quantum jumps, is applied to an arbitrary initial state in an anharmonic quartic potential,

$$V(x)=\tfrac{1}{2}(x^2+kx^4)\ . \tag{64}$$

Note that this potential provides an exact description of the quantum effects within the quasiclassical approximation as all higher-order terms vanish. The problem is first studied in two-dimensional phase space to validate the technique with exact solutions calculable by standard numerical techniques. The power of the technique developed herein lies in its direct applicability to higher dimensions and to many-particle systems.

The initial Wigner functions are chosen from a class of functions represented by

$$f(x,p,0)=2e^{-\beta[(x-x_0)^2-(p-p_0)^2]}\ , \tag{65}$$

such that $f_W=\beta f$, where the parameter β defines arbitrary admixtures of states. For examples considered here $x_0=0$ and $p_0=1$. See Figs. 7(a) and 7(b) for $\beta=0.25$. With $\beta=1$, the Wigner function corresponds to a

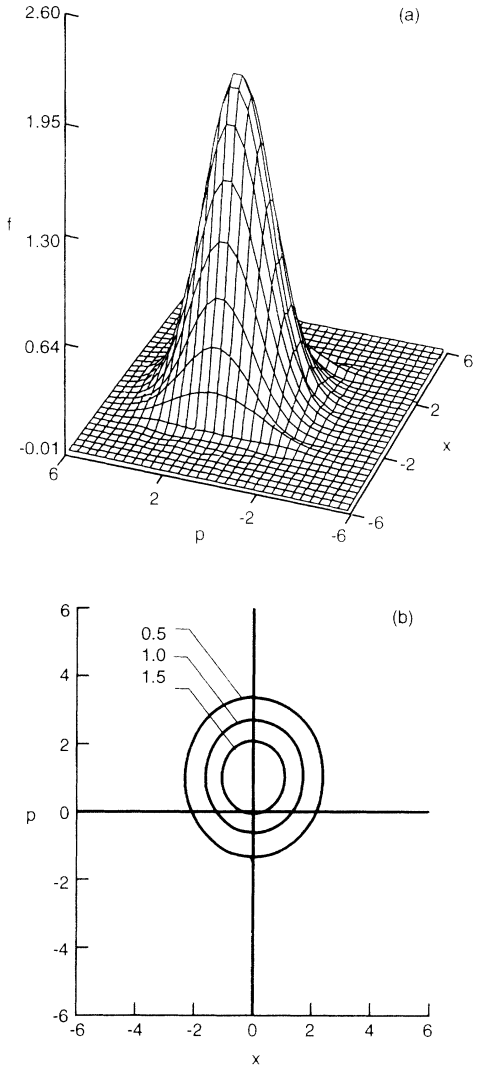

FIG. 7. Typical initial function f with (b) contours at levels 0.5,1.0,1.5 for $\beta=0.25$.

minimum wave packet which is a pure state [see Eq. (7)]. For $\beta<1$ the function therefore describes a mixture of states. Obviously $\beta>1$ is not allowed because of the uncertainty relations $\Delta x\,\Delta p \geq \frac{1}{2}$.

The Monte Carlo algorithm

The algorithm is based on the following complex of procedures. The initial set of δ functions is assigned to a fine mesh of phase-space grids. Using C-Language capabilities, a list of structures is constructed, each structure containing the data corresponding to the coordinates of the grid, the density, and the sign of the test points. Only the nonempty grids form the list. For the classical motion, with mass $m=1$, the coordinate data are updated using a two-step second-order Runge-Kutta method. This computation can be as accurate as desired, and does not involve a grid approximation. A high degree of accuracy is essential for the classical motion.

To implement the quantum event, all test points within a particular region in position space having all possible momentum values are identified by sorting. (To facilitate sorting, the list is constructed at two levels. The first level consists of structures for a coarse x grid and forms the main trunk. From each unit on the trunk a branch containing all the structures that fall within that unit is attached. The second-level structures contain the actual data.) The selected set is then allowed to undergo one-dimensional quantum jumps (see Sec. III A). The cumulative distribution for $F_{\pm}(a;p)$ is tabulated for various values of a. The required value of a is computed at the coarse x-grid location, via $a=V'''(x)\Delta t/24$. The net sum of newly formed test points are attached to the main list. The entire x space is spanned in this manner. With low creation probabilities and annihilation of pairs of opposite signs within the assigned grid spacing (annihilation distance) for the quantum motion, the main list does not increase exponentially and remains tractable.

With $N=20\,000$ the initial list size is ~ 4000 growing to a size of $\sim 15\,000$ at the end of $t=4\pi$, where each time unit π was subdivided into 30 time steps. The enhancement factor was chosen as $M=5$ and the grid size (annihilation distance) set at 0.3. The test points were given Gaussian width $\alpha'=0.4$. The function is reconstructed from the test points at the required time intervals using a suitable set of orthonormal harmonic-oscillator functions. On a micro VAX 4000 series the run time for the $0-\pi$ time segment was typically 5 min and approximately 40 min for $0-4\pi$ due to the increasing list size.

An earlier version of the algorithm was written in PL/I language. One complicated feature of the algorithm was to keep track of four nearest neighbors of a moving sample test point in order to facilitate sorting and annihilations of the newly created pairs, with their nearest neighbors having opposite signs. The algorithm developed here has proven to be faster and more accurate.

V. RESULTS AND DISCUSSIONS

Snapshots of the motion at time intervals in units of π are shown in Figs. 8–10 for various initial Wigner functions and for various strengths of the potential. The results are compared with the exact solution and also with the solutions of the classical Liouville equation.

The following observations can be made regarding the classical versus quantum motions. For the classical motion, the volume of phase space occupied by the system, an integral invariant of Poincaré, remains constant [15], but streams out into all phase-space regions allowed by energy conservation, developing whorls and tendrils [see Fig. 10(a)]. After long intervals of time this spread gives the appearance of a uniform distribution over a coarse grid, though finer grids would reveal the fine detail of the contour levels as shown in Figs. 8(a)–10(a). For the quantum motion, however, the system maintains a cohesiveness as the unit oscillates within the potential well. This cohesion may be the result of quantum interference effects arising from the oscillations of the Airy functions, causing cancellations and reinforcements over the classical motion.

Quantitative differences between pure-state ($\beta=1$) and mixed-state ($\beta<1$) quantum motions are also evident. For the pure-state motion, it may be observed that the

maximum height of the Wigner function remains unchanged. However, the mixed-state motion shows a "quantum focusing" effect as the Wigner function peaks beyond its initial maximum. Clearly, classical motion does not allow for such effects due to the Liouville theorem, which states that the density of systems in the neighborhood of some given system in phase space remains constant in time [15]. For more examples see Ref. [16].

Finally, as an example of computation of an observable, the averages for x and p are shown in Fig. 11, where

$$\langle x \rangle = (2\pi)^{-1} \int dx\, dp\, f_W(x,p,t) x \ , \tag{66}$$

$$\langle p \rangle = (2\pi)^{-1} \int dx\, dp\, f_W(x,p,t) p \ . \tag{67}$$

Averages are plotted for the purely classical and the ap-

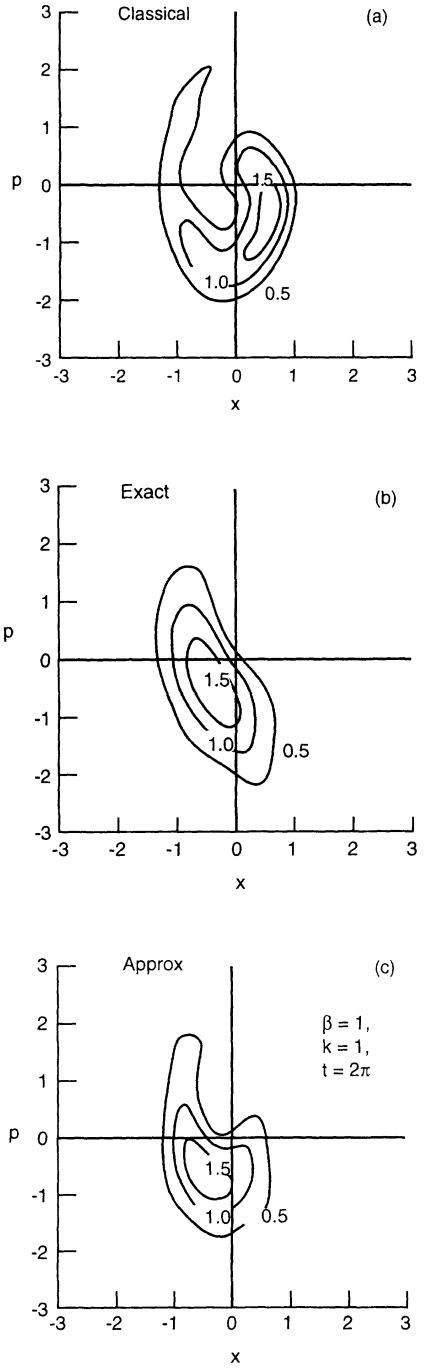

FIG. 8. Evolution of the Wigner function, f_W/β, in an anharmonic-quartic potential, $V(x)=\frac{1}{2}(x^2+kx^4)$, where $k=1$, $\beta=1$ for a pure state. $\alpha'=0.3$; grid size $=0.3$. The contour levels at $0.5, 1.0, 1.5, \ldots$, are at time $t=2\pi$. (a) Evolution via the classical Liouville equation. (b) Exact solution of the quantum Liouville equation. (c) Approximate evolution via the quantum Liouville equation.

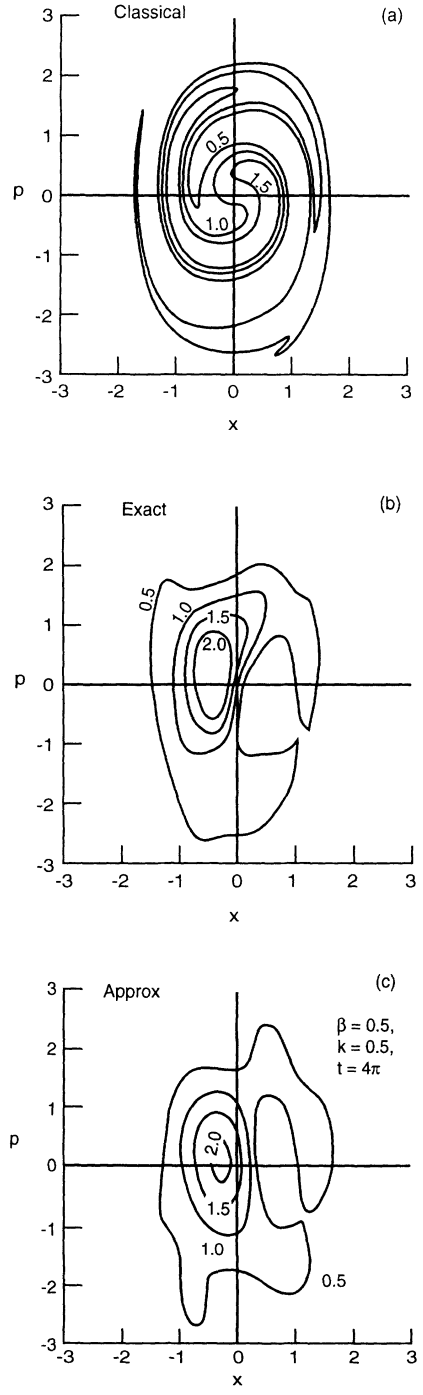

FIG. 9. Same as in Fig. 8 with $k=0.5$, for a mixed state $\beta=0.5$, at $t=4\pi$.

proximate quantum motion. For the classical motion the system distributes uniformly around the equilibrium point, consistent with energy conservation, and the first moments of the distribution tend to zero. For the quantum motion, however, these moments are oscillatory with finite amplitude, indicating a preservation of structural unity over long intervals of time.

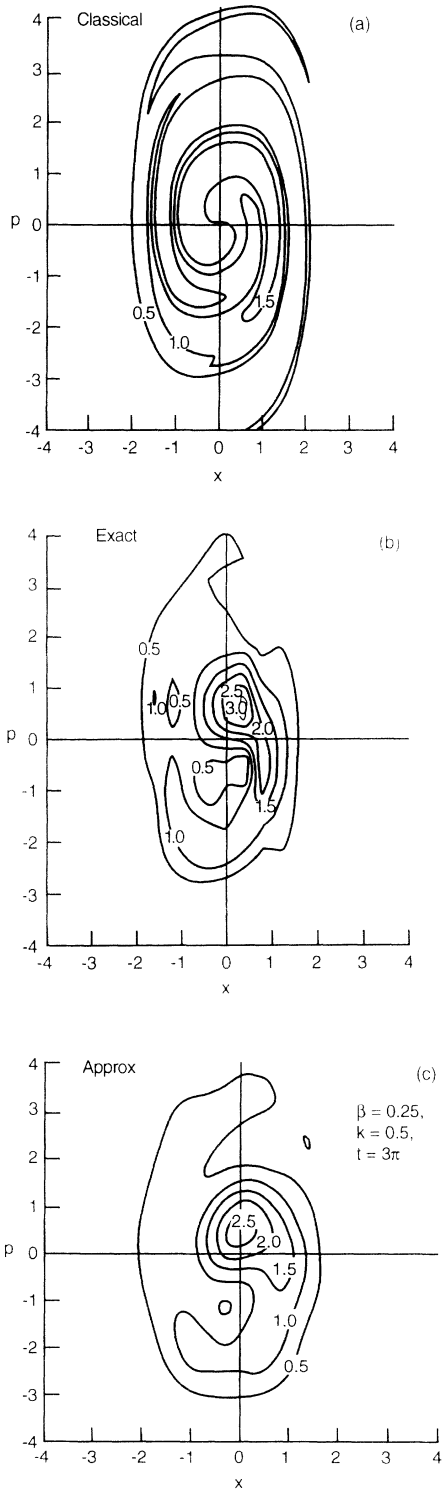

FIG. 10. Same as in Fig. 8 with $k=0.5$, for a mixed state $\beta=0.25$, at $t=3\pi$.

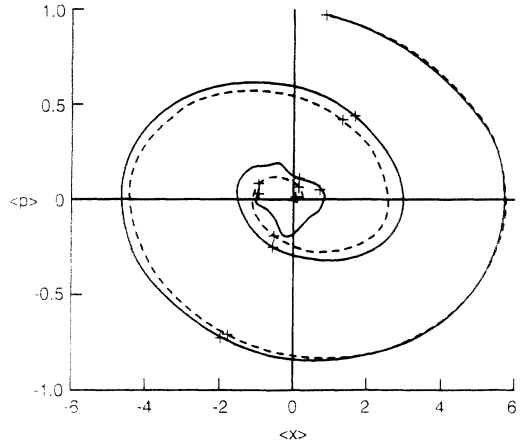

FIG. 11. First moments of the Wigner distribution function $\langle x\rangle,\langle p\rangle$, with $k=0.5$, $\beta=0.5$, over a period of time $0-4\pi$. Dashed line is for classical, solid line for approximate motion, with + marks at equal intervals of time.

Note added. A recent publication [17] applies the stochastic technique to low-energy heavy-ion collisions. Apparently, in that paper, extension to higher dimensions involves additional numerical computation. The technique detailed in this paper uses a simpler method to extend to higher dimensions which is fully applicable to the problem treated in Ref. [17].

ACKNOWLEDGMENTS

We acknowledge useful discussions with Professor E. A. Remler on topics relating to this work. Author S. John is grateful for NASA support under Contract No. NAS1-19237 and hospitality during the course of this work.

APPENDIX A

To evaluate

$$Q=V(r)(\vec{\nabla}_{\mathbf{x}}\cdot\vec{\nabla}_{\mathbf{p}})^3\delta(\mathbf{p})$$
$$=V(r)\frac{1}{(2\pi)^3}\int_{-\infty}^{\infty}(\vec{\nabla}_{\mathbf{x}}\cdot\mathbf{y})^3 e^{i\mathbf{p}\cdot\mathbf{y}}d\mathbf{y}$$

in terms of $\|^l$ and $\perp^r$ components,

$$\nabla_{\mathbf{x}}\equiv\left|\hat{\mathbf{e}}_r\partial_r,\hat{\mathbf{e}}_\perp\frac{\partial_\perp}{r}\right|,$$

$$\mathbf{y}\equiv(\hat{\mathbf{e}}_r y_\parallel,\hat{\mathbf{e}}_\perp\mathbf{y}_\perp).$$

Using the relations

$$\partial_\perp y_\parallel=\mathbf{y}_\perp,\quad \partial_\perp\mathbf{y}_\perp=-y_\parallel,$$

gives

$$(\nabla_{\mathbf{x}}\cdot\mathbf{y})V(r)=V'y_\parallel,$$

$$(\nabla_{\mathbf{x}}\cdot\mathbf{y})^2V(r)=V''y_\parallel^2+\frac{V'}{r}\mathbf{y}_\perp^2,$$

$$(\nabla_{\mathbf{x}}\cdot\mathbf{y})^3V(r)=V'''y_\parallel^3+3\partial_r\left|\frac{V'}{r}\right|y_\parallel\mathbf{y}_\perp^2;$$

therefore,

$$Q=\frac{1}{(2\pi)^3}\int_{-\infty}^{\infty}\left[V'''y_{\parallel}^3+3\partial_r\left[\frac{V'}{r}\right]y_{\parallel}y_{\perp}^2\right]e^{ip\cdot y}dy$$
$$=\left[V'''\partial_{p_{\parallel}}^3+3\partial_r\left[\frac{V'}{r}\right]\partial_{p_{\parallel}}\partial_{p_{\perp}}^2\right]\delta(\mathbf{p}) .$$

APPENDIX B

The expression to be evaluated is

$$\mathcal{J}_\alpha(a;p)=e^{-a\partial_p^3}\delta_\alpha(p) ,$$

where

$$\delta_\alpha(p)=\frac{1}{\sqrt{2\pi}\alpha}e^{-p^2/2\alpha^2} .$$

The results are presented [9].

1. Series expansion for $a << 1$

Using the series expansion for $e^{-a\partial_p^3}$ and applying the Rodrigues formula,

$$\mathcal{J}_\alpha(a;p)=\delta_\alpha(p)\sum_{n=0}^{\infty}\frac{a^n}{n!(\sqrt{2}\alpha)^{3n}}H_{3n}\left[\frac{p}{\sqrt{2}\alpha}\right] ,$$

where H is the Hermite polynomial.

2. Asymptotic evaluation for $p\to\infty$

The expression is rewritten using the integral representation for a Gaussian function,

$$\delta_\alpha(p)=\frac{1}{\sqrt{2\pi}\alpha}\int_{-\infty}^{\infty}dy\,e^{i\sqrt{2}py/\alpha-y^2} .$$

This gives

$$\mathcal{J}_\alpha(a;p)=\mathrm{Re}\frac{\sqrt{2|p'|}}{\pi\alpha}\int_0^{\infty}dy\exp\left[|p'|^{3/2}\left[ia'y^3-\frac{y^2}{\sqrt{|p'|}}\pm iy\right]\right] ,$$

where

$$p'=\left[\frac{\sqrt{2}}{\alpha}\right]p,\quad a'=\left[\frac{\sqrt{2}}{\alpha}\right]^3a .$$

The integral is evaluated by the method of steepest descent in the complex plane. Defining

$$f(z)=ia'z^3-\frac{z^2}{\sqrt{|p'|}}\pm iz ,$$

where z is a complex number, the saddle points occur at

$$z_0=\frac{-2i}{6a'\sqrt{|p'|}}[1\pm(1+3a'p')^{1/2}] .$$

The integral is evaluated independently for the following cases, along different paths of constant phase, and the resulting expressions are

$$\mathcal{J}_\alpha(a;p)=\begin{cases}\mathrm{Re}\dfrac{1}{\sqrt{2\pi}\alpha}e^{|p'|^{3/2}f(z_0)}\displaystyle\sum_{n=0}^{\infty}\frac{(ia')^n\Gamma[(3n+1)/2]}{n!|1+3a'p'|^{(3n+1)/4}}, & 1+3a'p'>0\\ \mathrm{Re}\dfrac{\sqrt{2}}{\pi\alpha}e^{|p'|^{3/2}f(z_0)+i\pi/4}\displaystyle\sum_{n\ \mathrm{even}=0}^{\infty}\frac{(ia'e^{3i\pi/4})^n\Gamma[(3n+1)/2]}{n!|1+3a'p'|^{(3n+1)/4}}, & 1+3a'p'<0 .\end{cases}$$

In the region $(1+3a'p')\sim 0$, with $3a'p'<0$, the expressions are

$$\mathcal{J}_\alpha(a;p)=\begin{cases}\mathrm{Re}\dfrac{\sqrt{2}}{3\pi\alpha}e^{|p'|^{3/2}f(z_0)+i\pi/6}\displaystyle\sum_{n=0}^{\infty}\frac{[-(1+3a'p')^{1/2}e^{i\pi/3}]^n\Gamma[(2n+1)/3]}{n!a'^{(2n+1)/3}}, & 1+3a'p'>0\\ \mathrm{Re}\dfrac{\sqrt{2}}{3\pi\alpha}e^{|p'|^{3/2}f(z_0)}\displaystyle\sum_{n=0}^{\infty}\frac{(1+3a'p')^{n/2}\Gamma[(2n+1)/3]}{n!a'^{(2n+1)/3}}[e^{i(n+1/2)\pi/3}+e^{i(n+1/2)\pi}], & 1+3a'p'<0 .\end{cases}$$

[1] U. Fano, Rev. Mod. Phys. **29**, 74 (1957).
[2] E. Wigner, Phys. Rev. **40**, 749 (1932).
[3] P. Carruthers and F. Zachariasen, Rev. Mod. Phys. **55**, 245 (1983).
[4] K. Imre, E. Ozizmir, M. Rosenbaum, and P. F. Zwiefel, J. Math. Phys. **8**, 1097 (1967).
[5] E. A. Remler, Ann. Phys. **95**, 455 (1975).
[6] J. R. Nix and D. Strottman, Phys. Rev. C **23**, 2548 (1981).
[7] J. W. Wilson, L. W. Townsend, W. Schimmerling, G. S. Khandelwal, F. Khan, J. W. Nealy, F. A. Cucinotta, L. C. Simonsen, J. L. Shinn, and J. W. Norbury, NASA Reference Publication No. 1257, 1991 (unpublished).
[8] T. B. Smith, Physica **100A**, 153 (1980).
[9] S. John, Ph.D. dissertation, College of William and Mary, 1986.
[10] S. John and E. A. Remler, Ann. Phys. **180**, 152 (1987).
[11] M. V. Berry and N. L. Balazs, J. Phys. A **12**, 625 (1979).
[12] J. V. Lill, M. I. Haftel, and G. H. Herling, Phys. Rev. A **39**, 5832 (1989).
[13] E. J. Heller, J. Chem. Phys. **65**, 1289 (1976); **67**, 3339

(1977).
[14] M. Hillery, R. F. O'Connell, M. O. Scully, and E. P. Wigner, Phys. Rep. **106**, 121 (1984).
[15] H. Goldstein, *Classical Mechanics* (Addison-Wesley, Reading, MA, 1950).
[16] S. John and J. W. Wilson, NASA Report No. TP3408, 1994 (unpublished).
[17] A. Bonasera, V. N. Kondratyev, A. Smerzi, and E. A. Remler, Phys. Rev. Lett. **71**, 505 (1993).

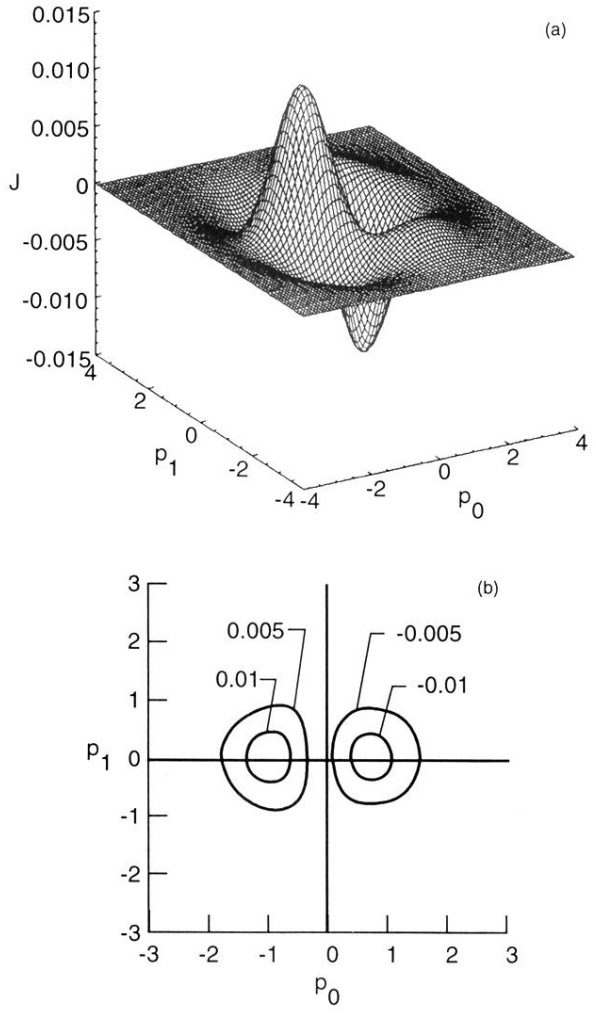

FIG. 4. (a) Analytic two-dimensional jump function $J_\alpha(a;p_0,p_1)$ with (b) contours for $a=0.1$, $\alpha=1$.